

CONF-820824-4

UCRL 87190

PREPRINT

An Absolutely Calibrated Soft-X-ray
Streak Camera for
Laser-Fusion Applications

R. L. Kauffman
H. Medeck
and
G. Stradling

This paper was prepared for submittal to
the 15th International Congress
on High Speed Photography
and Photonics
San Diego, CA

August 22-27, 1982

MASTER



Lawrence
Livermore
National
Laboratory

This is a preprint of a paper intended for publication in a journal or proceedings. Since changes may be made before publication, this preprint is made available with the understanding that it will not be cited or reproduced without the permission of the author.

DISTRIBUTION OF THIS DOCUMENT IS UNLIMITED

An Absolutely Calibrated Soft-X-ray Streak Camera
for Laser-Fusion Applications*

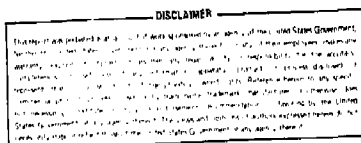
UCRL--B7190

DE82 018397

Robert L. Kauffman, Hector Medeck, and Gary Stradling**

Lawrence Livermore National Laboratory
Livermore, Ca 94550

Abstract



We have calibrated the intensity output of a soft-x-ray streak camera (SXRSC) in order to make absolute flux measurements of x rays emitted from laser-produced plasmas. The SXRSC developed at LLNL is used to time-resolve x-ray pulses to better than 20 ps. The SXRSC uses a Au photocathode on a thin carbon substrate which is sensitive to x rays from 100 eV to greater than 10 keV. Calibrations are done in the dynamic mode using a small laser-produced x-ray source. The SXRSC is calibrated by comparing its integrated signal to the output of calibrated x-ray diodes monitoring the source strength. The measured SXRSC response is linear over greater than two orders of magnitude. Using these calibrations, absolute intensities can be measured to an accuracy of $\pm 30\%$.

*Work performed under the auspices of the U.S. Department of Energy by Lawrence Livermore National Laboratory under contract # W-7405-ENG-48.

**Present address: Los Alamos National Laboratory, Los Alamos, N.M.

I. Introduction

X Ray streak cameras¹ are valuable instruments for diagnosing laser fusion plasmas. Their good time resolution (< 20 psec) and large dynamic range have allowed detailed temporal measurements of various spectral features of laser-produced x rays. Combined with x ray imaging elements, x-ray streak cameras have also been used to perform one-dimensional, time-resolved imaging². In these applications only relative intensity measurements have been made. In order to make quantitative measurements we have developed a method for calibrating x-ray streak cameras. Quantitative measurements of the soft x-ray spectrum have been important for understanding laser absorption and energy transport in laser-fusion targets³. These measurements are usually done using windowless x-ray diodes⁴ (XRD's) which can provide accurate quantitative information but with only moderate temporal resolution (> 200 psec) even using the most advanced oscilloscope technology⁵. For better time resolution in this x-ray region we have developed a soft x ray streak camera which is sensitive to x rays below 100 eV. Coupled with a suitable system for spectral discrimination this instrument is capable of making absolute flux measurements with an order of magnitude better time resolution than present XRD systems. A description of the calibration required for absolute measurements are presented here along with a brief description of the streak camera. With such an instrument absolute flux measurements to better than +30% appear feasible.

11. Instrument

The soft x ray streak camera⁶ (SXRSC) as shown in Figure 1 is similar in design to optical and other x-ray streak cameras developed at LLNL⁷. The SXRSC uses an RCA C73435A image converter tube whose schematic is shown in Figure 2. The photocathode is biased at -17 kV with an open extraction grid 5 mm wide biased at -14.5kV placed 4 mm from the cathode. The rest of the electron optics and deflection systems are identical to the other LLNL cameras. The sweep speed is nominally operated at 120 ps/mm and is independently calibrated before being fielded. Output is on a fiber optic coupled P-20 phosphor. The image is amplified using an 40 mm diameter ITT 4113 microchannel plate intensifier. The intensifier has a uniformity over its total area of better than +30% using a 3 mm aperture.

Image recording is done using either film or a CCD active readout system⁸. Film data is recorded on Kodak Royal X Pan. On each piece of data, a stepwedge is exposed using a calibrated flashlamp filtered to approximate the P-20 phosphor spectrum. Stepwedge data is used to convert film density to light exposure. By including it on each piece of data errors due to variations in film processing are reduced. With film, dynamic ranges of over 1000 are obtainable. Alternately, real time data recovery can be done using a 512x320 charge coupled device (CCD) system. The CCD is an RCA 52501 buried channel chip which has a pixel size of $30 \mu\text{m} \times 30 \mu\text{m}$. A fiber optic minifier reduces the image by a factor of three matching it to the size of the CCD. The image is recorded using 8 bit digitization. Taking into account background and noise in the CCD this system provides a dynamic range of about 100. This can be increased by increasing the number of digitization bits.

The unique feature of this camera is its thin window cathode sensitive to soft x rays. Previous x ray streak cameras have used 8 μm -25 μm Be windows as photocathode substrates¹. Such thick windows were required because the image converter tubes were sealed and the windows had to withstand atmospheric pressure. In the soft x ray version the image converter tube is actively pumped using an ion pump allowing a much thinner cathode substrate to be used. For our initial experiments, which are described here, the cathode substrate is a 50 $\mu\text{g}/\text{cm}^2$ vapor deposited carbon foil which is 25% transparent at 100 eV. For future experiments we plan to use a 10 $\mu\text{g}/\text{cm}^2$ parylene substrate. This CH thin film has a 75% transmission at 100 eV. For these quantitative measurements the photocathode material is a 300 \AA thin film of Au. These films are relatively stable for these applications and are around 5% efficient in the soft x ray region⁹.

III. Quantitative Measurement

Quantitative measurements can be made using the SXRSC by correlating the signal out to the x-ray flux incident on the slit. If F_x is the incident x-ray flux, it is related to the SXRSC signal, s , by the expression

$$s = \frac{d \xi \epsilon \gamma}{m_x m_t v_s} \eta F_x, \quad (1)$$

where d is the entrance slit width and v_s is the sweep speed of the camera at the output image. η is the photocathode conversion efficiency. The image converter tube dependent quantities are the electron transmission efficiency, ϵ , image magnification along the slit

and in the time direction, m_x and m_t , respectively, and the electron to light conversion efficiency of the phosphor, ξ . γ is the detector efficiency for either film or CCD readout averaged over the P-20 phosphor output and includes losses in coupling to the image converter tube. The SXRSC response depends on x-ray energy primarily through the photocathode conversion efficiency, η . The electron signal from the photocathode is due to secondary electrons created by the stopping of an energetic electron produced by photoabsorption in Au. The secondary electron spectrum has been shown to be independent of incident photon energy¹⁰. All of the parameters besides η can be combined in a single proportionality constant, α , that depends only on the parameters of the instrument and not on the x ray energy. Equation 1 can be rewritten

$$s_x = \alpha \eta_x F_x \quad (2)$$

where the subscripts denote explicitly the dependence on x ray energy.

Quantitative calibrations require the determination of the proportionality constant, α in Eq. 2. Quantum efficiencies for Au and other possible photocathode materials have been measured for x ray energies greater than 100 eV⁹. Therefore, determination of α requires only measurement of the incident x-ray flux and the resultant SXRSC signal.

IV. Experiment

For calibration of our soft x ray streak camera we use a laser-produced plasma as a soft x ray source. Figure 3 is a schematic of our experimental arrangement. Pulses which are 50 ps-150 ps of 1.06 μm

laser light irradiate at normal incidence slabs of various materials. Irradiance energies vary from 100 mj to 1 joule producing x-ray pulses whose widths are on the order of the incident laser pulse. The intensity of the x-ray pulses are monitored using windowless XRD's at 45° with respect to the incident laser direction. The soft x-ray streak camera views the target also at 45° with respect to the incident laser direction on the side opposite the XRD's.

The laser-produced spectra from these targets are, in general, a continuum in the subkilovolt region with prominent line or band emission from highly stripped ions. In order to achieve moderate energy discrimination for SXRSC, three sets of x ray transmission filters and mirrors are used. These channels along with their mean energy and channel width are listed in Table I. The relative shape of the three x ray channels are shown in Figure 4 including the energy dependence of the photocathode. The thickness of the filter is chosen to provide a region of high transmission below the K- or L-absorption edge whose energies are listed. The absorption in the foil continues to rise at lower energies providing a low energy cutoff by such techniques a resolving power $E/\Delta E \sim 3-5$ is obtainable. The x ray mirrors act as a low pass filter chosen to suppress higher energy x rays above the absorption edge where the filter becomes transparent. Similar filters are used with the XRD's to cover the same energy bands these channels are also shown in Figure 4. No x ray mirrors are used with the XRD's which, along with the difference in cathode response, accounts for the difference in shape. The differences are especially apparent in the high energy portion of the spectrum.

The x-ray mirrors and filters as well as the XRD's are calibrated at

two x ray sources off line. Below 0.9 keV a 300 keV proton beam is used to produce characteristic K and L-x rays which provides a D.C. line source for measuring the x-ray mirror reflection efficiency and filter transmission at well defined discrete energy points. Examples of the calibrations for an x ray mirror and filter transmission are shown in Figures 5 and 6, respectively. Above 0.9 keV, a bremsstrahlung continuum source coupled with a Si(Li) detector having less than 0.2 keV resolution is used to measure the fall off of the mirror reflectivity. The solid curve in Figure 5 is an empirical fit to the data using semi-classical calculations of the reflectivity.

Estimates of the source spectrum can be made from the three XRD channels. These estimates are shown in Figure 7 for several targets. Medium and low Z targets show much structure in their spectrum while high Z targets of Ta and Au show little structure. High resolution spectra have been taken of several medium Z targets ($Z=21-24$) in the energy range from 500 eV - 700 eV and are shown in Figure 8. Many lines observed are due to ionized L-shell transitions. Such structure can introduce uncertainties in the calibration since the channel responses of the SXRSC do not exactly match the XRD channel responses. If a strong line in the spectrum occurs where the two channel responses greatly differ, the ratio of the signals from the two instruments will show large excursions from the ratio expected for a flat or smoothly varying spectrum.

V. Data Analysis

As shown in Section III, calibration of the SXRSC requires relating

the SXRS signal to the incident x-ray flux. Since the x ray flux is continuous over the x ray spectrum, Eq. 2 must be integrated over x ray frequency, or

$$S_{SX} = \Omega_{SX} \alpha \int R_{SX}(E) F(E) dE \quad (3)$$

where Ω_{SX} is the solid angle of the slit. R_{SX} includes the cathode response, η . If R_{SX} is averaged over the incident spectrum then Eq. 3 can be written

$$S_{SX} = \Omega_{SX} \alpha \bar{R}_{SX} \bar{F} \Delta E \quad (4)$$

where ΔE is the average width of the channel. \bar{R}_{SX} and $\bar{\Delta E}$ can be calculated from the channel responses in Figure 4 assuming a spectral shape. The average responses and widths for the three channels are listed in Table I. A similar analysis can be done for the XRD data to derive the average fluence values F .

An example of the correlation of the SX signal versus average fluence for the iron channel is shown in Figure 9. The data fall along a straight line through the origin although there appears to be a systematic deviation upon the target. The deviations are probably due to differences in the x-ray spectrum as discussed earlier. The data has a mean deviation of 25% for all target types. Variations within a single type of target is less than 10%. Similar analysis has been performed for the other two channels. The results for all three are listed in Table II. The units relate the signal from the camera output (bits are units of CCD digitization) to the current density (e^-/cm^2-ps) from the photocathode. The errors reflect the variations in α for different

targets. α appears to decrease as the mean channel energy is increased from 200 eV for the carbon channel to 650 eV for the iron channel although the mean of the three are within errors of each value. The lowest energy channel suffers most from variations of the spectrum reflected by the large errors. Such deviations would indicate that the energy dependence of the secondary electron distribution is not energy independent.

Several cathodes similar to the one calibrated here have also been calibrated. Their calibrations agree within 30%. The variation is probably due to sample to sample variations in the thickness of the Au layer or carbon substrate. The variations may also indicate changes of the Au secondary electron efficiency during its shelf life. No auxilliary measurements have been made of their secondary electron efficiency to correlate with their calibrations. In the future, such correlations would be useful.

The sensitivity of these instruments is excellent as seen from the calibration factor. One resolving element in the CCD corresponds to a detection region of 100 μm by 100 μm at the photocathode and a temporal window of 10 psec. The calibration factors indicate this corresponds to about 4 electrons from the photocathode per bit in the CCD which approaches the quantum limit for detection. The calibration factors are a function of all of the parameters discussed in Section III including image intensifier gain.

VI. Conclusion

In summary we have performed intensity calibrations of an x-ray

streak camera capable of measurements down to 100 eV. Such an instrument can be used to make quantitative measurements of the x-ray flux which is important for diagnosing laser fusion targets. The intensity calibrations indicate that such an instrument can approach the quantum limit of sensitivity. We are continuing our efforts to improve the errors in the calibrations which appear to be in part due to the source spectral distributions. We also plan to extend the detection region to lower energies by using a thinner cathode substrate. A thinner substrate would also reduce discontinuities around the carbon K-edge. These changes would improve the calibration and the instrument utility for measuring x-ray flux.

DISCLAIMER

This document was prepared as an account of work sponsored by an agency of the United States Government. Neither the United States Government nor the University of California nor any of their employees, makes any warranty, express or implied, or assumes any legal liability or responsibility for the accuracy, completeness, or usefulness of any information, apparatus, product, or process disclosed, or represents that its use would not infringe privately owned rights. Reference herein to any specific commercial products, process, or service by trade name, trademark, manufacturer, or otherwise, does not necessarily constitute or imply its endorsement, recommendation, or favoring by the United States Government or the University of California. The views and opinions of authors expressed herein do not necessarily state or reflect those of the United States Government thereof, and shall not be used for advertising or product endorsement purposes.

References:

1. C. F. McConaghy and L. W. Coleman, *Appl. Phys. Lett.* 25, 268 (1974);
L. Coleman and D. Attwood, Laser Program Annual Report-1974, edited
by J. I. Davis, (Lawrence Livermore National Laboratory, Livermore,
CA, UCRL-50021-74, 1974) pp 315-319.
2. D. T. Attwood, L. W. Coleman, M. J. Boyle, J. T. Larsen,
D. W. Phillion, and K. R. Manes, *Phys. Rev. Lett.* 38, 282 (1977);
R. H. Price, Laser Program Annual Report, Vol. 2, , edited by
L. Coleman, (Lawrence Livermore National Laboratory, Livermore, CA,
UCRL-50021-79, 1979) pp 5-54 tp 5-57.
3. M. D. Rosen, D. W. Phillion, V. C. Rupert, W. C. Mead, W. L. Kruer,
J. J. Thompson, H. N. Kornblum, V. W. Slivinsky, G. . Caporaso,
M. J. Boyle, and K. G. Tirsell, *Phys. Fluids* 22, pp 2020-2031 (1979).
4. K. G. Tirsell, H. N. Kornblum, and V. W. Slivinsky, *Bull. Amer. Phys.*
Soc. 23, 807 (1978); Lawrence Livermore National Laboratory
UCRL-81478 (1979).
5. K. A. Lerche and D. E. Campbell, Laser Program Annual Report, Vol. 2,
edited by L. Coleman (Lawrence Livermore National Laboratory,
Livermore, CA, UCRL-50021079, 1979) pp. 5-2 to 5-4.
6. G. L. Stradling, M. S. Thesis, Brigham Young University, 1981.
Lawrence Livermore National Laboratory Report No. UCRL-52568.

7. S. W. Thomas, G. R. Tripp, and L. W. Coleman, Proceedings of the 10th International Congress on High Speed Photography, edited by E. Larion (Assoc. Nat. de la Recherche Technique, Paris, France, 1972) pp. 127-133; S. Thomas, J. Houghton, T. Owen and L. Coleman, Laser Program Annual Report 1974, edited by J. I. Davis (Lawrence Livermore National Laboratory, Livermore, CA, UCRL-50021-74, 1974) pp. 292-296.
8. J. Cheng, G. Tripp and L. Coleman, International Conference on the Application of CCD Devices (San Diego, CA, 1978).
9. B. L. Henke, J. P. Knauer, and K. Premaratne, J. Appl. Phys. 52, 1509-1520 (1981).
10. B. L. Henke, J. A. Smith and D. T. Attwood, J. Appl. Phys. 48, 1852-1866 (1977).
11. R. W. Kuckuck, J. L. Gaines, and R. D. Ernst, Proceedings of the 4th Conference on Scientific and Industrial Applications of Small Accelerators, edited by J. Daggan and I. L. Morgan, (IEEE, Piscataway, N.J., 1976) p. 229.

Figure Captions

1. Photograph showing the soft x ray streak camera as mounted on the LLNL Shiva laser facility. This unit is equipped with a CCD active readout system for prompt data recovery and analysis.
2. A schematic of the LLNL x-ray streak camera. The principal component is an RCA image converter tube. Recording can be done either on film as shown here, or using a CCD active readout detector.
3. A schematic of the set up for the x ray streak camera calibration.
4. A comparison of the channel response of the SXRSC with that of the XRD used for the calibration. The components of the channels are listed in Table I.
5. Calibration of the x ray mirrors used with the SXRSC. The symbols are measured values. The curves are empirical fits to the data using a semi-classical theory for the reflectivity.
6. Measured transmission of the x ray filters used in the calibrations. The symbols are the data. The curves are fits to the data using published x ray absorption cross sections.
7. Examples of the output spectra used in the calibration for various x ray targets. The data is reduced from the three channels of XRD data. Large variations in the spectra are observed depending on the target material.

8. High resolution spectra for several different target materials. Positions of known lines for the various ionization states are marked. Differences in the x ray spectra can affect the SXRSC calibrations.

9. Example of calibration data for the 500-700 eV channel. The SXRSC signal is plotted versus x ray fluence in this region as measured by the XRD. Some systematics are noted depending in the x ray spectrum. Overall, the data correlate a mean value indicated by the straight line.

TABLE 1. SXRS Channel Characteristics

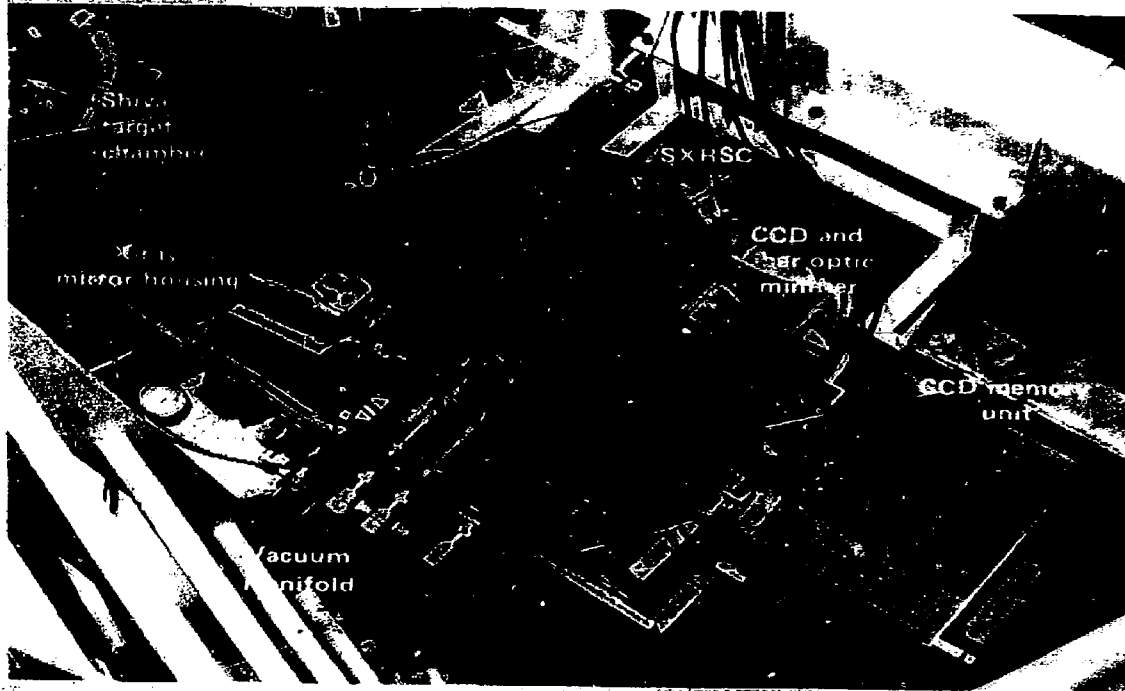
Filter	Mirror	\bar{E}	ΔE	\bar{R}
Carbon 100 $\mu\text{g}/\text{cm}^2$	Carbon 5°	195 eV	70 eV	$3.0 \times 10^{-2} \text{ e}^-/\text{keV}$
Vanadium 280 $\mu\text{g}/\text{cm}^2$	Nickel 5°	403 eV	240 eV	$4.1 \times 10^{-3} \text{ e}^-/\text{keV}$
Iron 300 $\mu\text{g}/\text{cm}^2$	Nickel 3°	590 eV	260 eV	$1.1 \times 10^{-2} \text{ e}^-/\text{keV}$

TABLE II. Average Calibrations for SXRSC

Target	$\alpha, 10^{-4}$ bits/(e ⁻ /cm ² -ps)		
	Carbon	Vanadium	Iron
Ta	4.8 <u>+0.9</u>	3.2 <u>+0.6</u>	2.3 <u>+0.2</u>
Au	5.3 <u>+0.5</u>	2.9 <u>+0.7</u>	2.1 <u>+0.3</u>
V	1.8 <u>+0.1</u>	-- --	1.3 <u>+0.2</u>
Fe	2.8 <u>+0.3</u>	-- --	-- --
Average	3.7 <u>+1.7</u>	3.0 <u>+0.5</u>	1.9 <u>+0.5</u>

Mean Calibration factor = 2.5×10^{-4} bits/(e⁻/cm²-ps)
+0.4

SXRSC SPECTROMETER AS MOUNTED AT SHIVA



40-30-0181-0250

Figure 1

SCHEMATIC OF THE LLL STREAK CAMERA

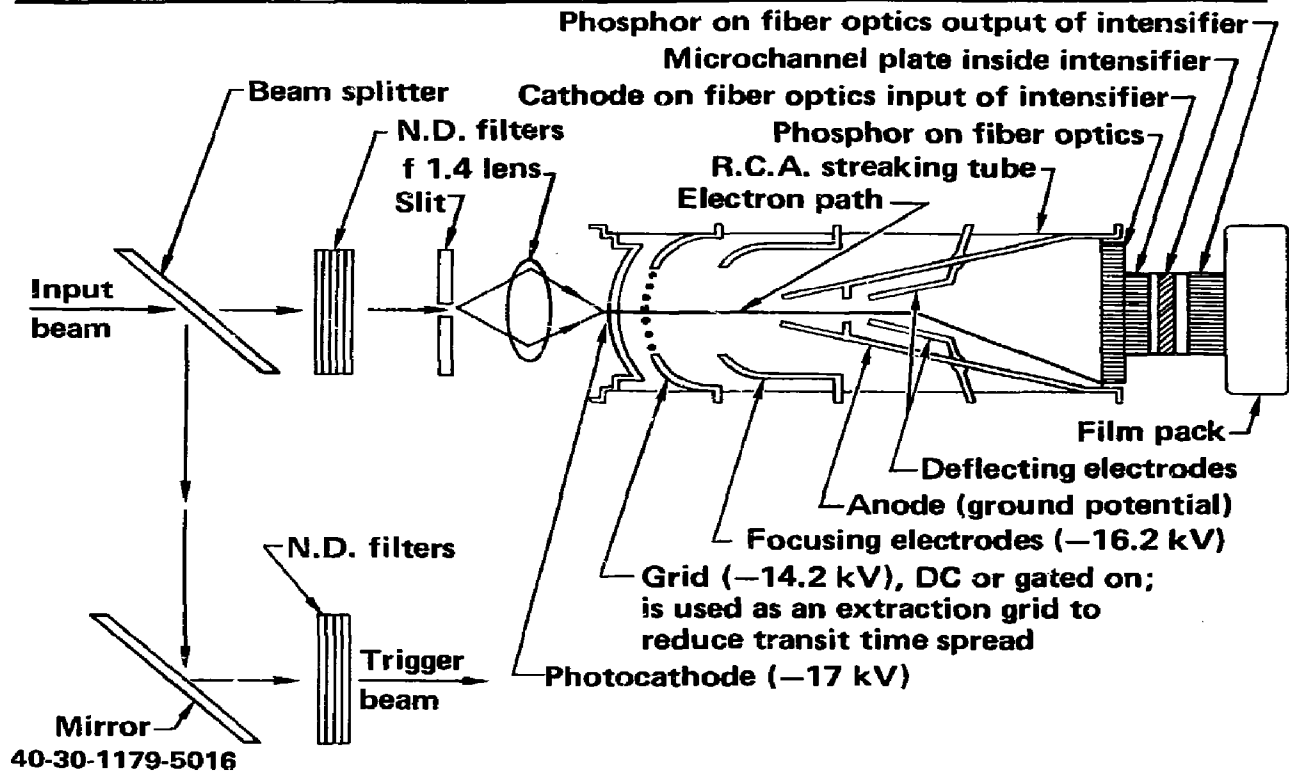
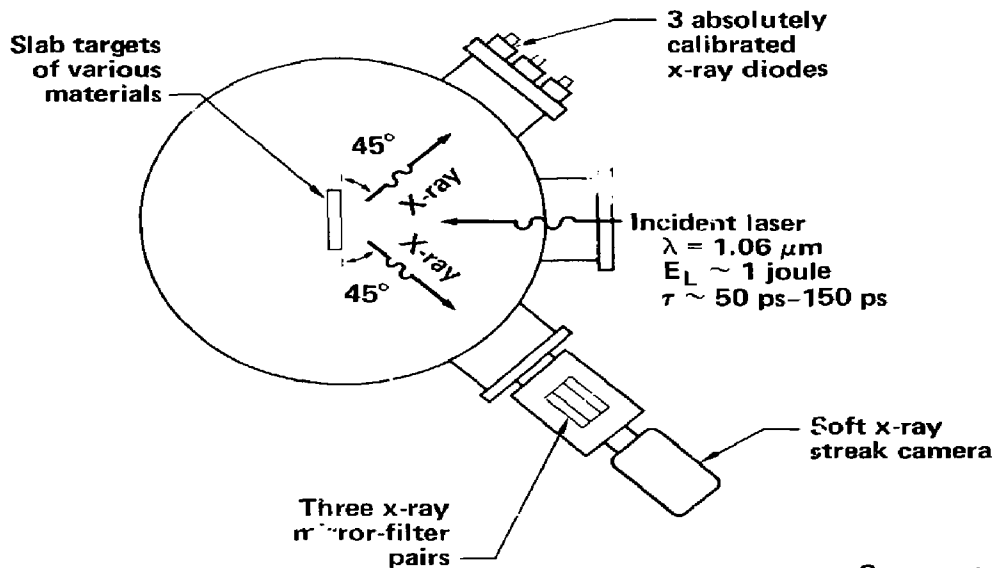


Figure 2

THE SXRSC IS CALIBRATED USING A LASER-PRODUCED PULSED X-RAY SOURCE



A schematic of the calibrations



The SXRSC calibrations

- Are done in the dynamic mode using 70-170 ps x-ray pulses
- Use a broad band x-ray source with $h\nu < 1$ keV
- Use transmission filters to define three coarse x-ray channels
- Are done by comparing x-ray fluences measured by calibrated x-ray diodes (XRD's) to the integral signal from the SXRSC

$$S_{\text{SXRSC}} \approx \frac{\bar{R}_{\text{SXRSC}} \Delta E_{\text{SXRSC}}}{\bar{R}_{\text{XRD}} \Delta E_{\text{XRD}}} S_{\text{XRD}}$$

40-30-0581-1276

Figure 3

COMPARISON OF CHANNEL RESPONSE

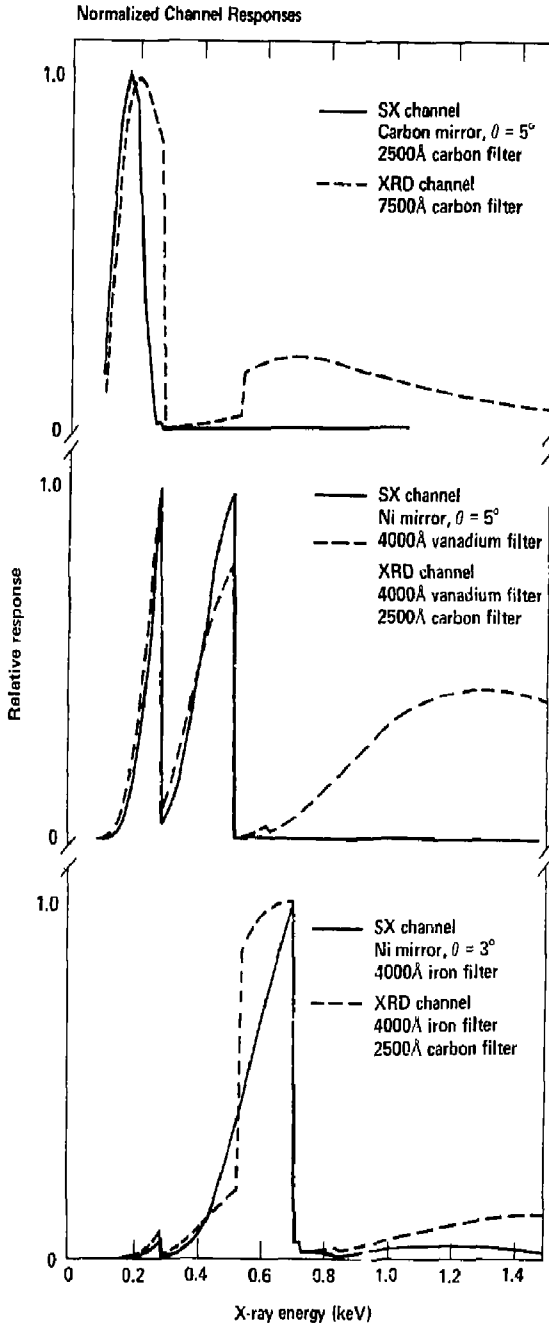
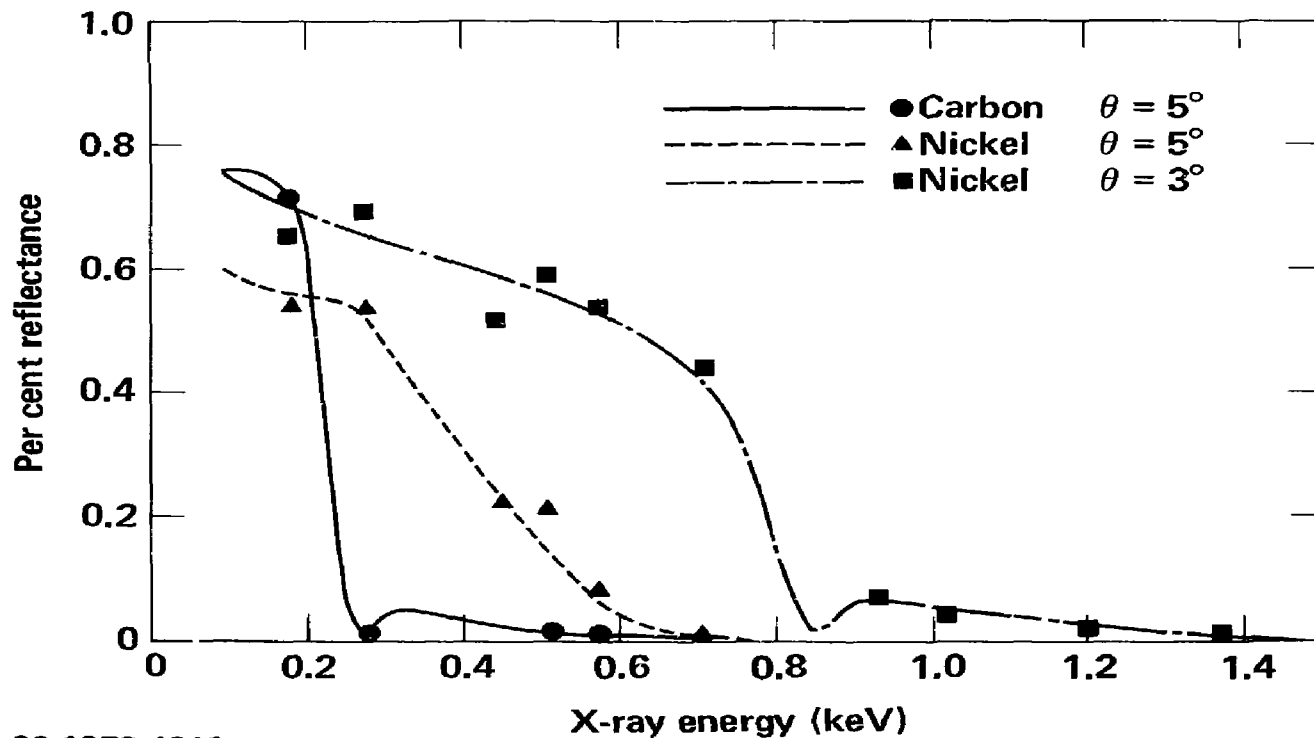


Figure 4

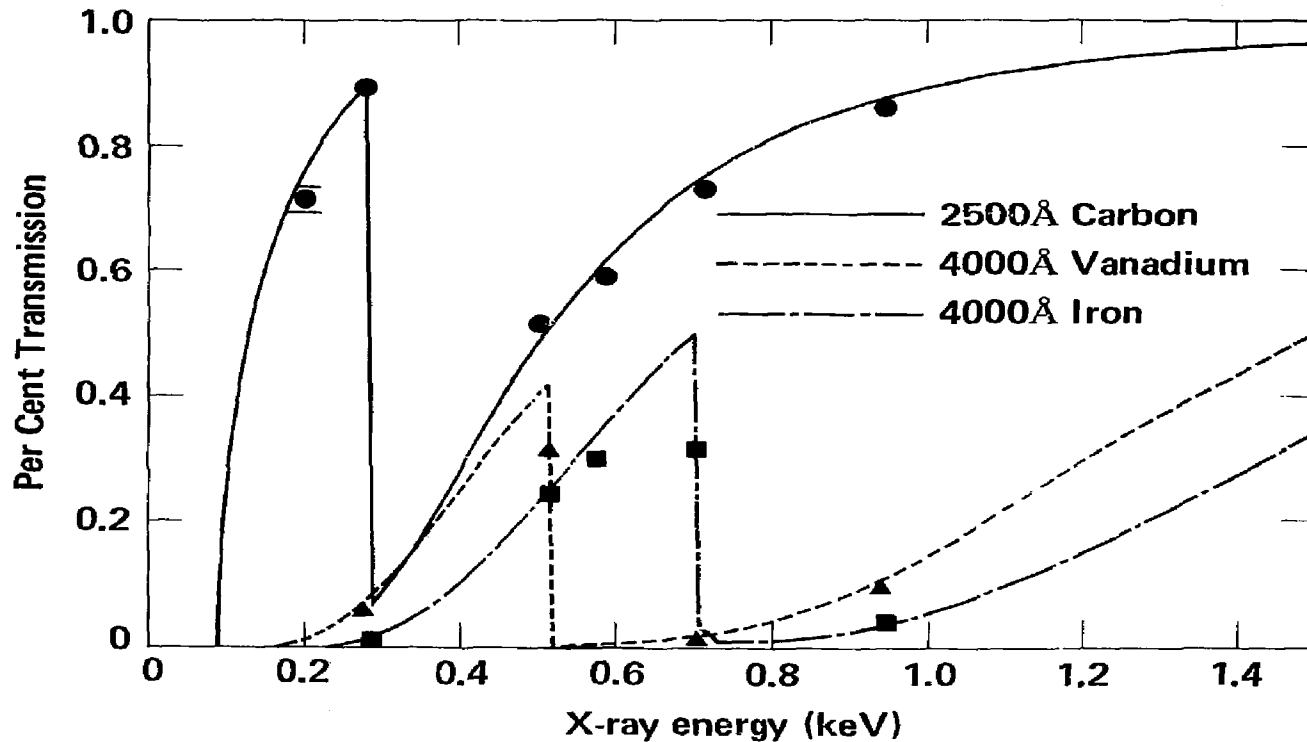
CALIBRATION OF THE X-RAY MIRRORS FOR THE SXRSC CHANNEL



40-90-1079-4913

Figure 5

MEASURED FILTER TRANSMISSION



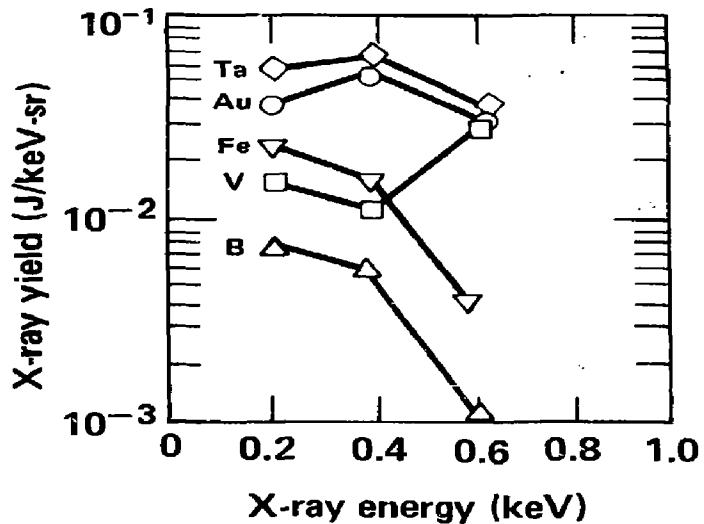
40-90-1079-4914

Figure 6

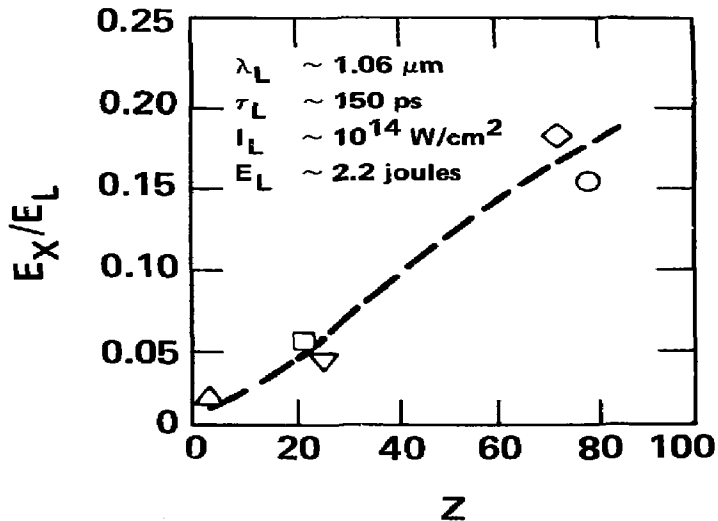
X-RAY SOURCE SPECTRA AT THE MONOJoule DEPEND ON THE TARGET MATERIAL



X-ray spectra from various targets



X-ray conversion efficiency

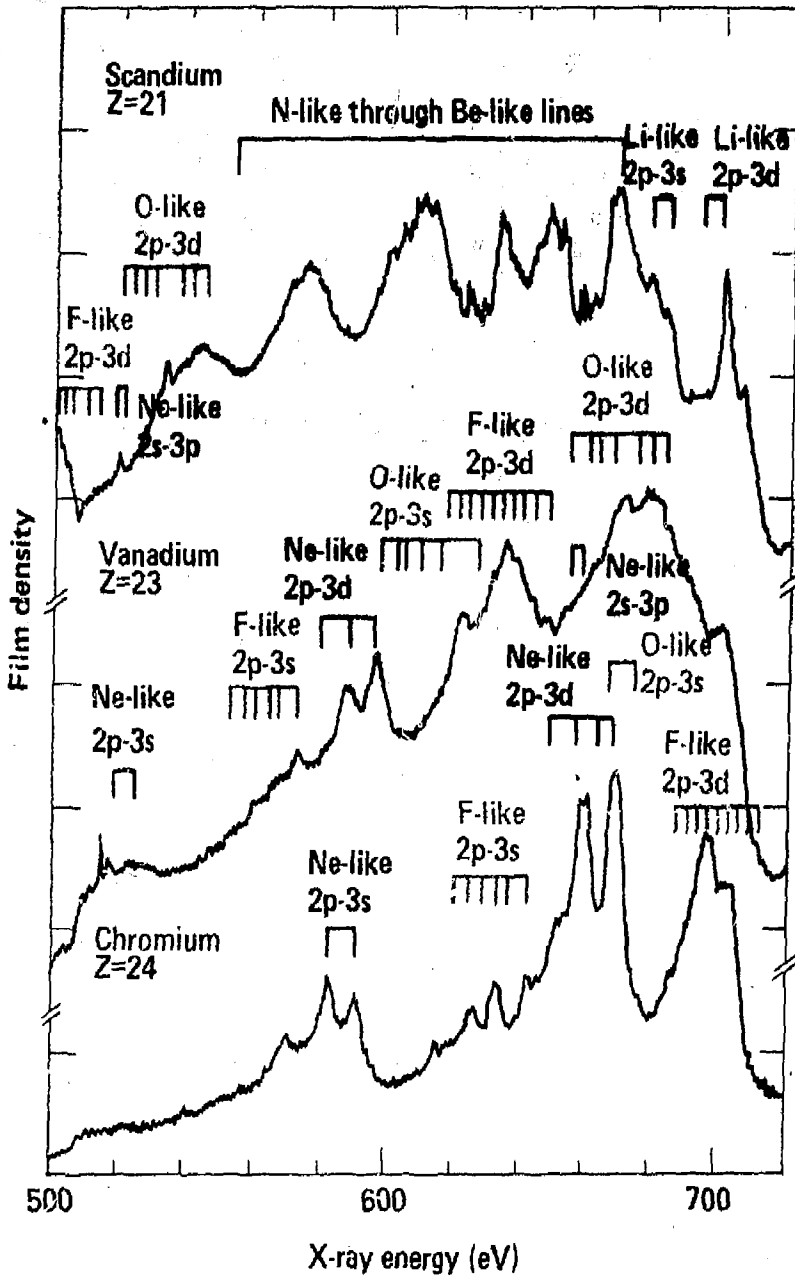


40-90-0581-1374

6/81

Figure 7

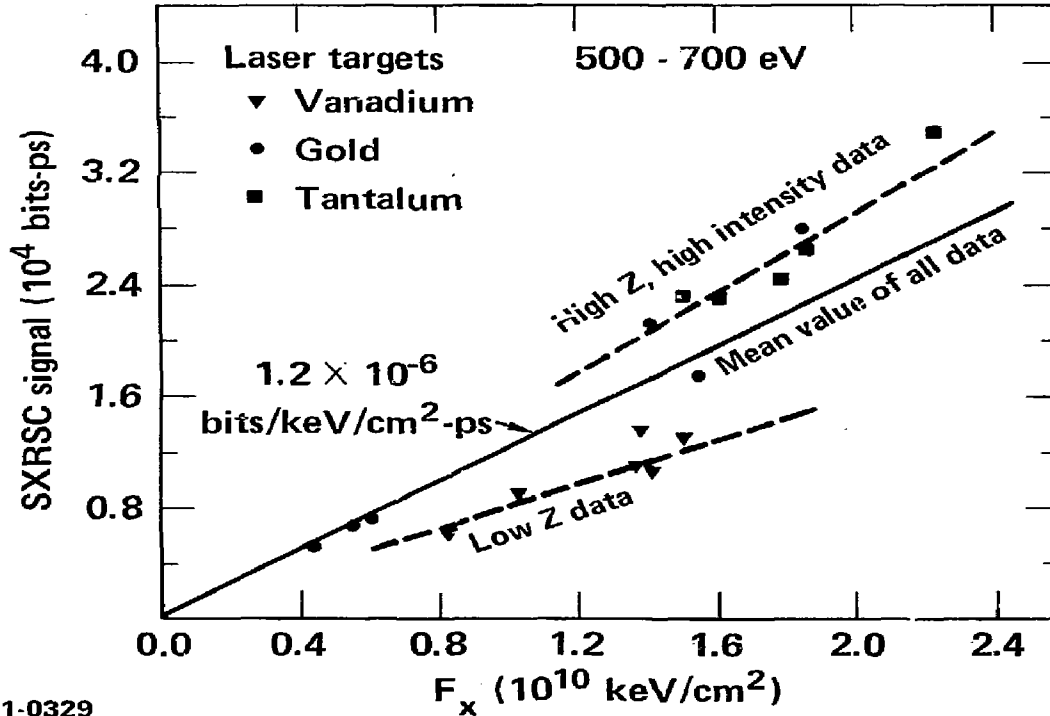
Laser produced X-ray spectra from slab targets on the monojoule



40-90-0181-0045

Figure 8

SXRSC CALIBRATIONS OF THE MONOJoule VARY DEPENDING ON TARGET SOURCE SPECTRUM



40-90-0281-0329

Figure 9